2008

Electrochemical deposition of bismuth telluride thermoelectric nanowires

Raymond Harry, III Scheffler
San Jose State University

ELECTROCHEMICAL DEPOSITION OF BISMUTH TELLURIDE THERMOELECTRIC NANOWIRES

A Thesis

Presented to

The Faculty of the Department of Chemical and Materials Engineering

San Jose State University

In Partial Fulfillment

of the Requirements for the Degree

Master of Science

by

Raymond Harry Scheffler, III

August 2008

APPROVED FOR THE DEPARTMENT OF CHEMICAL AND MATERIALS ENGINEERING

Melanie McNeil 7-2-08

Dr. Melanie McNeil

Qi Laura Ye 7-2-08

Dr. Qi Laura Ye, Eloret, NASA ARC

Guna Selvaduray 7-2-08

Dr. Guna Selvaduray

APPROVED FOR THE UNIVERSITY

Thea L. Williamson 07/18/08

ABSTRACT
ELECTROCHEMICAL DEPOSITION OF BISMUTH TELLURIDE
THERMOELECTRIC NANOWIRES

by Raymond Harry Scheffler, III

Bismuth telluride and tellurium rich bismuth telluride wires of diameters of 35, 55, 73, and 200 nm and lengths of up to 50 microns were synthesized through constant current electrochemical deposition for thermoelectric applications. Aqueous solutions with pH values of 0.5 and 1, and -0.1 and -0.5 mA currents were used in a design of experiments matrix for electrodeposition into templates with 200 nm diameter pores and approximately 1 cm^2 surface area. Analysis of variance showed that the change in current had the greatest effect on the growth rates of the 200 nm diameter wires. Qualitative composition characterization indicates that the -0.5 mA current setting and pH 1 solutions lead to higher tellurium concentrations in the wires, and a similar trend was also found to be true for the 35, 55, and 73 nm nanowire runs. In probe measurements, wires from each set of deposition conditions demonstrated n-type behavior.

ACKNOWLEDGEMENTS

Several people and entities were critical to the completion of this thesis. The author would like to thank Dr. Melanie McNeil at SJSU and Dr. Qi Laura Ye at NASA for their guidance. Additional thanks are due to his lab mates and coworkers at NASA, particularly Jyoti Kumari, Ryan Leverenz, and Hidenori Yamada. Dr. Toshige Yamada was gracious in helping interpret probe measurements and electron diffraction data. Dr. Roger Terrill and Dr. Paul Pak of SJSU's Department of Chemistry were very kind in running samples through their ICP. And lastly, the author would like to thank his friends and family, particularly his parents and "little brother" and "little sister."

TABLE OF CONTENTS

LIST OF FIGURES

LIST OF TABLES

CHAPTER ONE

INTRODUCTION

Between 1820 and 1850, the fundamental concepts of thermoelectrics, the forming of a temperature gradient from a current or the generation of a current from a temperature gradient, were first investigated and exploited in such inventions as the thermocouple and the thermoelectric pile [1]. After a long period of relative inactivity in thermoelectric research, the 1940's and 1950's brought about the thermoelectric materials that would be predominantly incorporated into the thermocouples, thermoelectric coolers and low-power generators of the next half-century [1]. Generally, these thermoelectric devices have been more inefficient and costly than traditional methods of cooling and power generation. The reliability of having no moving parts and the unavailability of readily useable energy have prompted the utilization of this technology in space and a few specialized markets. Within the past decade, the emergence of nanotechnology, environmental concerns regarding refrigerant chemicals, and interests in the supercooling of electronics has brought about yet another resurgence of investigation in this field and the possibility of new applications [1, 2].

A current is generated from a temperature gradient when the heated charge carriers of p-type and n-type legs of a thermoelectric device are driven towards the cold end of the temperature gradient. Conversely when a potential is applied, the charge carriers create a temperature gradient by flowing in the opposite direction. The upper limit to this phenomenon is the Carnot efficiency. As real systems fail to accomplish this

thermodynamic ideality, the measure by which a material is suited for thermoelectric devices is called the figure of merit, ZT, and is given by

$$ZT = \frac{S^2\sigma}{\kappa}T \qquad \text{Equation 1}$$

where S is the Seebeck coefficient, T is temperature, and σ and κ are electrical and thermal conductivity, respectively. It should be noted that the parameter Z has units of inverse temperature and that Z multiplied by T constitute the dimensionless ZT.

As the ZT value of a material increases, the efficiency of the energy conversion reaches the Carnot limit. For the past four decades, commercial thermoelectric materials have had room temperature ZT values that have hovered just below 1 without much increase [1-3]. A ZT value of 1 is approximately equivalent to a Carnot efficiency of 10 percent. To be competitive with standard air compressor cooling, a thermoelectric device would need materials with ZT greater than 4, or 30 percent of Carnot efficiency [2].

Should improvements to the efficiency of energy conversion through nanotechnology be realized, thermoelectric devices could be incorporated into an untold number of portable gadgets such as biomedical implants. In the case of a pacemaker, a thermoelectric power source that utilizes the 3 to 4 ^{o}C difference between the skin and the core of the body could do away with the need to operate on patients to replace their drained pacemaker batteries. Conversely, thermoelectric heat sinks could be integrated into computer chips, refrigerators, and other temperature sensitive environments for cooling purposes.

Currently, there is a two-pronged approach to developing more efficient thermoelectric devices. Firstly, various novel materials are being investigated, and secondly, the dimensions of these materials are being reduced. Bismuth telluride (Bi_2Te_3) and bismuth telluride alloys with slight deviations in composition have been the standard room temperature thermoelectric materials since the 1960's [2]. Materials development had typically included investigating the crystal structures of bulk Bi_2Te_3, adjusting the atomic ratio of bismuth and telluride, substituting bismuth with antimony such as $(Bi_{1-x}Sb_x)_2Te_3$ and substituting tellurium with selenium such as $Bi_2(Te_{3-y}Se_y)$ where x and y are between 0 and 1. Other multi-component, non-Bi_2Te_3 materials have also been explored, and these include skutterudites, carbon nanotubes, and ternary alloys and superlattices. However, it is typically found that when the thermal conductivity of materials decreases, the Seebeck coefficient also decreases [4].

Decreasing the dimensions of a bulk, thermoelectric material to the nanoscale is predicted to increase its figure of merit as much as an order of magnitude. Materials contained within diameters less than their de Broglie wavelengths in all but one direction are considered effectively one dimensional. At the nanometer scale, there is an expected increase in the *S* value due to enhancement of density of states and an increase in the boundary scattering of phonons, the quantum vibrations by which heat is conducted in crystals. Growing and integrating nanowires with high *ZT* values into a thermoelectric device can exploit these quantum size effects.

There are, however, several challenges to growing and characterizing nanowires, wires with diameters between 1 nm and 100 nm. Firstly, manipulating matter into

diameters that are essentially only thousands of atoms and orienting and integrating the nanowires into devices are beyond the capabilities of standard microelectronics processing techniques. Secondly, verifying the composition and crystallinity of nanowires requires delicate sample preparation and special characterization equipment that can focus on small dimensions. These difficulties are compounded when trying to characterize the thermoelectric properties of the nanowires.

A combination of nanoscaling and material composition is investigated in this thesis as part of an effort to develop more efficient thermoelectric devices. Electrochemical deposition into mesoporous templates—pores of diameters in the submicron range and templates with pores of diameters less than 100 nm—was chosen as the method of synthesis for the bismuth telluride nanowires. Electrochemical deposition is relatively cheap, is performed mostly near ambient temperatures, and offers large coverage areas when compared with other growth methods such as those utilizing vapor-liquid-solid mechanisms or metal organic chemical vapor deposition [22]. Also, the reagents used in this method tend to be less toxic than those used in metal organic chemical vapor deposition.

Electrochemical deposition utilizes an electrochemical reaction to form a solid from an electrolyte solution containing dissolved species onto a conducting substrate, also known as the working electrode. The reaction can be driven by an applied voltage or an applied current; in the special case of electroless deposition, the reduction reaction is driven by an inherent potential difference between the electrode and electrolyte solution. For the electrochemical deposition of bismuth telluride, the reaction is

$$3\ HTeO_2^+ + 9\ H^+ + 18\ e^- + 2\ Bi^{3+} \rightarrow Bi_2Te_3\ (s) + 6\ H_2O \qquad \text{Equation 2}$$

when starting with an aqueous acid electrolyte solution. The reaction initially occurs at the solution/substrate interface at nucleation sites but continues at the interface of the deposited material and the electrolyte solution where charge can be transferred.

A non-conducting structure can be used to selectively block deposition from areas of the working electrode. One such structure is mesoporous anodic alumina, sometimes sold as anodic alumina membranes (AAMs) for filtration purposes. Figure 1 shows SEM images of the top and cross section of an AAM. The ordered regions of AAMs have arrays of pores arranged hexagonally, with domains similar to a honeycomb's structure. The pores of the AAMs can be tuned to diameters between tens and hundreds of nanometers with a narrow pore size distribution within any single AAM. The pores can also be made to have high aspect ratios with lengths in the tens of microns. The order, length, uniformity, and relative chemical stability of the pores of AAM templates are the main advantages for this application over other mesoporous materials such as track etch membranes and self assembled polymer membranes. The most glaring disadvantage to anodic alumina is that it is too thermally conductive to be used in the final thermoelectric device [48].

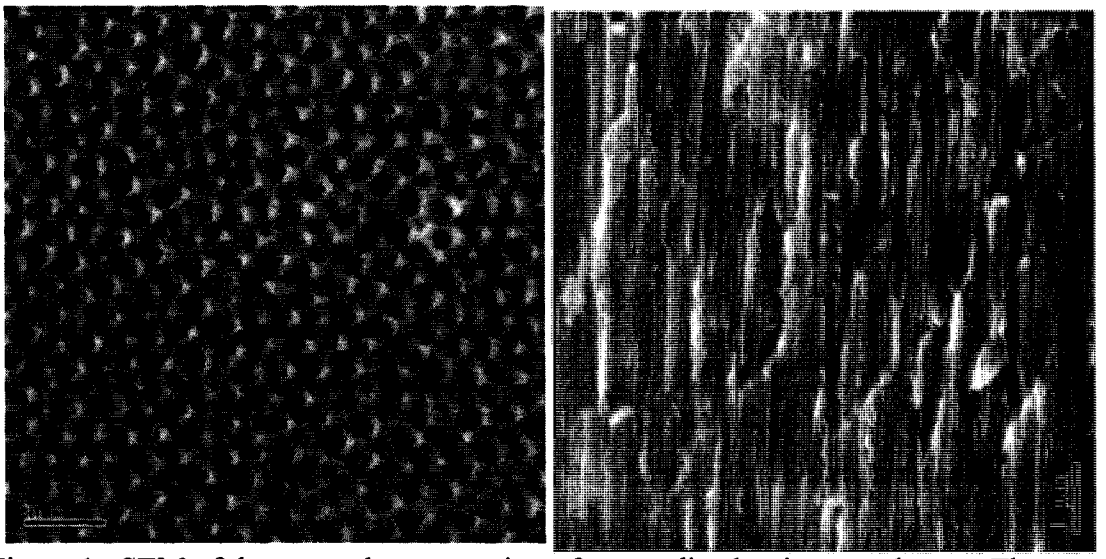

Figure 1. SEM of the top and cross section of an anodic alumina membrane. The cross section appears rough as this sample was simply snapped in half as opposed to being diced with a saw.

When one side of an AAM is coated with a metal film such as gold and the pores are filled with a deposition solution, this set up can take the place of a working electrode. The material deposited within each pore is confined; in this way, wires are grown. One of the advantages of templated electrochemical growth of nanowires for devices is that the wire must be connected to the bottom of the pore and continuous through the channel in order to grow [6]. As the pores are parallel, electrochemical deposition into AAMs can be used to create arrays of parallel nanowires. And though not attempted in this investigations, thermoelectric devices could be fabricated with regions of p and n type nanowire arrays through a series of steps involving lithography and electrochemical deposition with two sets of parameters [17, 18].

CHAPTER TWO

LITERATURE REVIEW

2.1 Aspects of Electrochemical Bi_2Te_3 and Alloy Nanowire Deposition

Several papers have been published on the synthesis of bismuth telluride and bismuth telluride alloy nanowires [5-21]. The majority of the publications reviewed on bismuth telluride nanowire synthesis describe the electrochemical deposition from an aqueous nitric acid solution into anodic alumina membranes (AAMs) that serve as templates [5-19]. Other methods published include electrochemical step edge decoration and vapor phase growth via laser ablation [20-21].

2.1.1 Electrochemical Deposition

A review of work on the electrochemical deposition of bismuth telluride films gives insight into the electrochemical deposition of bismuth telluride nanowires without the complications added by nanoporous templates. Without the use of a template, the electrochemical process of depositing bismuth telluride and its alloys would take the form of thin films. Several researchers have studied variations on the electrochemical deposition of bismuth telluride thin films [24-31]. Zhu and coworkers write that concentrations of at least 0.001 M of $HTeO_2^+$ are only soluble in the pH range of -0.37 to 1.93 [29]. 1 M HNO_3 solutions in which Bi^{3+} and $HTeO_2^+$ are dissolved are often used to deposit thin films [24-29]. Although, two papers reviewed report using other acid solutions such as hydrochloric acid and perchloric acid with tartaric acid in their bismuth telluride and bismuth telluride alloy depositions [30, 31]. The concentrations of bismuth

and tellurium in the electrochemical solutions ranged from 0.0001 M to 0.02 M with varying ratios between the two components [24-29]. Microscopically rough films of various qualities were produced, and the films with better adhesion and greater crystallinity were reported for slower, lower voltage depositions [24-29].

It should be noted that Menkhe and coworkers have been able to kinetically control the deposition and stripping of bismuth telluride on highly ordered pyrolytic graphite edges to form nanowires in a template-free method termed step edge decoration [20]. The bismuth telluride preferentially nucleates and deposits at a feature on the electrode, in this case a straight edge that resembles a step [20]. This method can form a wire if the deposition is stopped prior to film formation, and reversing the polarity of the electrodes can result in etching to form thinner wires [20]. The multiple nucleation sites along the length of the wire grown by step edge decoration could prevent the formation of single crystal quality wires [20].

2.1.2 Nanoporous Templates

Unlike step edge decoration, electrochemically depositing nanowires in templates allows for the formation of nanowires perpendicular to the working electrode [5-18, 23]. Most researchers growing the bismuth telluride nanowires either purchased AAMs or produced them in house using a two step anodization method delineated by Masuda and Fukuda [5-18, 23]. Figure 2 is a schematic of this method. These templates are formed from aluminum foils that are first cleaned and sometimes polished [23]. The aluminum is then anodized in an acid solution—the recipe, applied voltage, and bath temperature vary

depending on the target pore size—and the alumina formed tends to arrange in a honey comb structure with high aspect ratio pores [5-18, 23]. When the alumina from this first anodization is selectively etched, the newly exposed aluminum is dimpled at the location of the former pore bottoms [23]. These dimples allow for the formation of a more ordered array of pores in a second anodization step [23]. Following a second anodization, the supporting aluminum can be removed with a mercury chloride or copper chloride solution [5-18, 23]. During anodization, a thin alumina layer forms at the interface of the pore bottom and the aluminum and is removed as a final step before the template is prepared for electrochemical deposition [23].

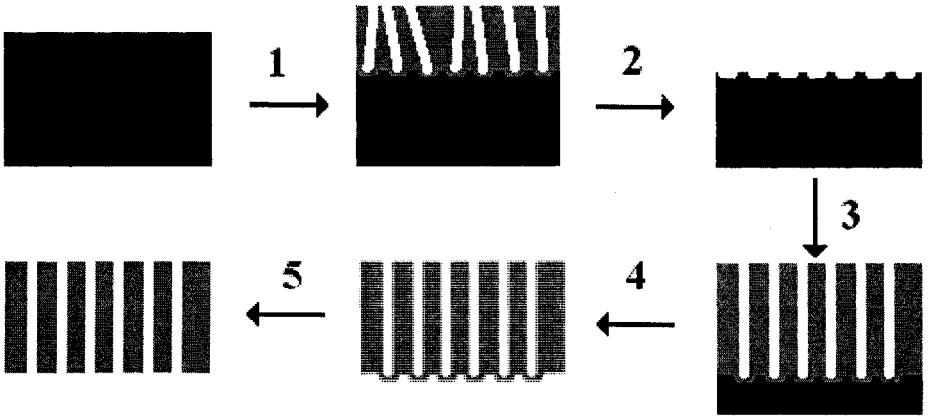

Figure 2. Schematic for the fabrication of AAMs with aluminum shown in black and alumina in grey. The steps are 1) first anodization, 2) alumina etch, 3) second anodization, 4) aluminum etch, and 5) pore bottom removal.

In a review of nanostructures created in templates, Huczko lists that a selected template should be wet by the deposition solution, withstand the conditions of deposition, and avoid blockage [22]. As such, there are limits to the deposition parameters in which AAMs meet these criteria. Sander and coworkers developed AAMs on substrates using a

single anodization process in which the final method for removing the barrier layer between the electrode and the pore channel was to soak the AAM in the 1 M HNO_3 deposition solution for half an hour prior to anodization [7]. This would be an indication that the AAM is susceptible to dissolution by a strongly acidic 1 M HNO_3 solution. Also of concern was the blocking of pores due to capping by overfilled pores whose wires had grown faster than their neighbors or by overfilled cracks in which the bismuth telluride preferentially deposited; as such relatively uniform growth is a key condition for a high yield of nanowires [7]. And for the diameters of pores investigated, capillary forces could impede the complete wetting of all of the pores with the deposition solution [5-18].

2.1.3 An Overview of Electrochemical Deposition of Bi_2Te_3 and Alloy Nanowires

A group lead by Martin, a pioneer in electrochemical deposition in anodic alumina membranes, was the first to report on the electrochemical deposition of bismuth telluride in porous templates [5]. Martin's wires were approximately 280 nm in diameter and 60 μm long and were cathodically deposited from a solution of 1 M nitric acid with 0.033 M bismuth and an estimated 0.025 M dissolved tellurium in the form of $HTeO_2^+$ [5]. The wires were grown at a current density of 3.5 mA/cm^2 from a gold film working electrode evaporated onto the AAM [5]. The working electrode was configured horizontally, and nitrogen was bubbled through the deposition solution [5]. The nanowires were released from the template after it was dissolved in 5 M sodium hydroxide and were determined to be composed of only bismuth and tellurium by energy dispersive x-ray spectroscopy [5].

Following Martin's work, Stacy's group has written several papers on the electrochemical deposition of bismuth telluride and bismuth telluride alloy nanowires [6-11]. Their work includes wires much below 100 nm, down to 24.5 nm [11]. They also report depositing alloys into AAMs to make p-type ($Bi_{1-x}Se_x$ and $Bi_{0.6}Sb_{1.6}Te_{2.8}$) and n-type ($Bi_2Te_{2.7}Se_{0.3}$) nanowires of various diameters [8-10].

A summary of the bismuth telluride deposition conditions is presented in Table 1. Table 2 contains a summary of the dimensions and composition of the bismuth telluride nanowires grown in these studies.

Table 1. Survey of the conditions used to deposit bismuth telluride nanowires. Duration and use of reference electrode were not reported in all papers.

Author	Deposition solution			Applied voltage or current	Duration
	[HNO_3]	[Bi]	[Te]		
Sapp [5]	1 M	0.033 M	0.025 M	-3.5 mA/cm^2	2 hours
Prieto [6]	1 M	0.01 M	0.01 M	-0.45 V vs. Hg/Hg_2SO_4 reference electrode	12-14 hours
Sander [7]	1 M	0.075 M	0.1 M	-0.46 V vs. Hg/Hg_2SO_4 reference electrode	--
Sander [11]	1 M	0.075 M	0.1 M	-0.46 V vs. Hg/Hg_2SO_4 reference electrode	--
Jin [13]	Buffered pH 1 solution	0.035 M	0.05 M	-2.5 mA/cm^2	2 hours
Li [14]	Buffered pH1 solution	0.01 M	0.015 M	-1.3 V pulse for 3 ms with 10 ms recovery	--
Wang [15]	1 M	0.013 M	0.01 M	-0.15 V vs. SCE	--
Xu [16]	1 M	0.075 M	0.1 M	-1.85 V	15 minutes

Table 2. Survey of the properties of bismuth telluride nanowires electrochemically deposited in alumina templates.

Authors	Wire diameter (nm)	Wire length (μm)	Compositional analysis
Sapp [5]	280 ± 30	60	XRD confirmed Bi_2Te_3
Prieto [6]	40	50	SEM EDS indicated 40 ± 5 atomic % Bismuth for large range of conditions
Sander [7]	45 ± 5	55	SEM EDS and XRD confirmed Bi_2Te_3
Sander [11]	24.5 ± 2.7 47.3 ± 7.5 74.6 ±3.1	--	SEM/TEM EDS indicated 40 atomic % Bi
Jin [13]	50	--	TEM EDS determined 54 atomic % Bi [19]
Li [14]	40 60	50	EDS confirmed Bi_2Te_3
Wang [15]	50	100	XPS confirmed Bi_2Te_3
Xu [16]	100	50	EMPA determined 40 ± 5 atomic % Bi

2.1.4 Electrochemical Deposition Conditions

The majority of the works reviewed utilized a 1 M HNO_3 solution with various concentrations of dissolved bismuth and tellurium [5-7, 11, 15-16]. Xu and Sander both reported using concentrations of 0.075 M Bi^{3+} and 0.1 M Te^{2+}, which are on the upper end for reported concentrations [7, 11, 16]. Prieto reports the lowest concentrations for bismuth and tellurium with 0. 01 M each [6]. Prieto elucidates that she was trying to reduce the available bismuth and tellurium to slow the growth of the nanowires and that the concentrations she reported were just above the limit at which gas formation occurs at the working electrode [6]. As such, Prieto has the longest growth time of the investigations reviewed [6].

Depositions were performed under constant voltage, constant current, and pulsed voltage regimes [5-7,11,15-16]. Martin and Jin reported using relatively similar constant current values for deposition at -3.5 and -2.5 mA/cm^2, respectively, despite Martin's having much larger pore diameters [5, 13]. In constant voltage investigations, Stacy's group reported using voltages of -0.45 and -0.46 V verses a Hg/Hg_2SO_4 reference electrode in their studies, and Wang used -0.15 V versus a saturated calomel electrode for reference [6, 7, 11, 15]. Xu reported -1.85 V with no reference electrode mentioned [16]. While there is some comparison between Wang and Stacy's voltages when taking into consideration that different reference electrodes were used, Xu's -1.85 V value seems quite high, and the deposition time of 15 minutes is much shorter than others [6, 7, 11, 15, 16]. Li reported using a -1.3 V pulse for 3 ms but also implemented a rest between pulses for 10 ms in order to slow deposition and allow for ion concentrations near the wire/solution interface to replenish [14].

2.1.5 Nanowire Properties

The dimensions of the nanowires grown in the papers reviewed are listed in Table 2. The diameters of the nanowires are determined by the diameter of the pores as the deposited bismuth telluride wet the walls of the pores [5-16]. The lengths of the wires match the thickness of the AAMs as growth was stopped when overgrowth was observed [5-16].

Though precise reporting of nanowire composition is lacking, a summary of the compositional analysis of the wires is also summarized in Table 2. Most papers only

confirmed the deposition of bismuth and tellurium in the pores with SEM EDS, TEM EDS, XRD, XPS, or EMPA and generally concluded that the wires were near the stoichiometric ratio within the error limits of the characterization tools [6, 7, 11, 15, 16]. Prieto reported that even within a wide range of changes in the deposition voltage and chemical concentrations the stoichiometry of the wires remained within 5 percent of 40 atomic percent bismuth and 60 atomic percent tellurium as determined by SEM EDS [6]. However, Shi and coworkers reported that Jin's nanowires were 54 atomic percent bismuth as determined by TEM EDS [19].

While other groups had reported polycrystalline wire growth, Jin and coworkers and Li and coworkers declared that their bismuth telluride nanowires were single crystalline [13, 14]. These researchers adjusted the pH of their deposition solutions; both report using solutions of pH 1 [13, 14]. Jin's constant current deposition approach resulted in wires that had XRD patterns indicating (110) and (220) peaks for hexagonal Bi_2Te_3, and Li's pulsed voltage deposition resulted in XRD patterns indicating (015) and (0210) for hexagonal Bi_2Te_3 [13, 14].

The composition and crystallinity of the nanowires had been reported, but the wires with significant thermoelectric enhancement have not been demonstrated. In two papers, Wang and coworkers grew arrays with wires 50 nm in diameter of n-type and p-type bismuth telluride with Seebeck coefficients of 270 μV/K and -188 μV/K, respectively [13, 15]. These measurements were taken for areas of nanowire arrays connected in parallel [13, 15]. The thermoelectric properties of individual nanowires grown by Jin and coworkers were measured in collaboration with Shi's group [19]. The

nanowires were reported to have a low ZT, around 0.02 at room temperature, due to the low Seebeck coefficient obtainable with a composition of $Bi_{0.54}Te_{0.46}$ [19]. An SEM image of Shi's suspended structure used to measure the thermoelectric properties of individual nanowires is shown in Figure 3.

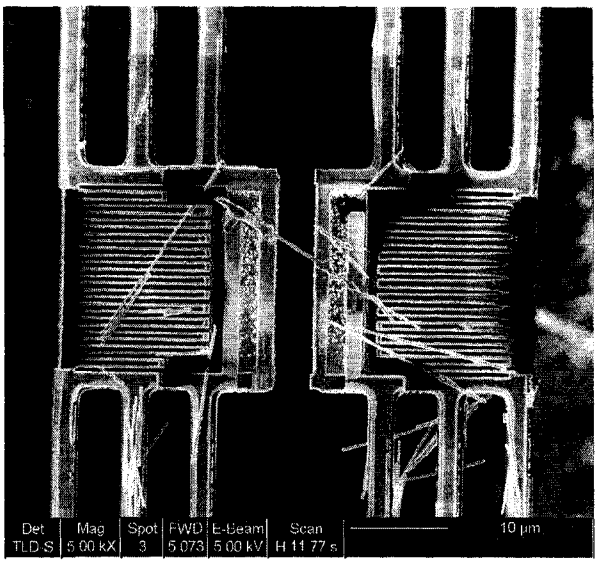

Figure 3. SEM image of microfabricated suspended structure used in making four-probe resistance, Seebeck coefficient, and thermal conductivity measurements. The nanowire being measured was dropped across the two pads shown in the picture.

2.2 Other Forms of Bismuth Telluride

Besides nanowires, other papers have been published on the synthesis of unique bismuth telluride materials. The highest figure of merit of any material published thus far has come from Venkatasubramanian and coworkers at Research Triangle Park [33]. They were able to produce thin films made of Bi_2Te_3/Sb_2Te_3 superlattices with room temperature *ZT* values of approximately 2.4 [33]. Venkatasubramanian was able to cool to 32 K from around room temperature using this new material [33]. In 2004, Service reported that Venkatasubramanian and coworkers expected to publish data indicating

their production of material with a *ZT* of around 3.5 [34]. Other work in bismuth telluride materials includes the sonochemical [35, 36], hydrothermal [37] and solvothermal synthesis [38] of nanocrystalline powders, but no thermoelectric properties were reported.

2.3 Indium Antimonide Nanowires

In 2004, Mingo suggested that indium antimonide would be a potential candidate for an increased figure of merit thermoelectric nanowire [39]. In a talk and subsequent papers, the efforts to grow indium antimonide nanowires at NASA Ames Research Center were reviewed [32, 40-42]. The InSb nanowires were grown using the vapor-liquid-solid mechanism, and these nanowires were not aligned and did not have dense coverage [32, 40-42]. Using a method similar to that reviewed in a previous section, Zhang and coworkers have reported on the electrochemical deposition of InSb nanowires into AAMs [43].

2.4 Other Thermoelectric Materials

There has been a wide range of work published on the investigations of new, multi-component, thermoelectric materials other than bismuth telluride alloys that are intended for various temperature ranges. Hsu and coworkers reported that their bulk $AgPb_{18}SbTe_{20}$ had a maximum *ZT* of 2.2 at 800 K [44]. While this measurement was taken at a temperature range that is not feasible for biomedical implants or household devices, this is the best *ZT* value given for materials for salvaging heat waste from

engines [44]. A notable room temperature thermoelectrics study is the work by Harman and coworkers in quantum dot superlattices [45]. Harmon and workers were able to synthesize PbSeTe/PbTe quantum dots with *ZT* values between 1.3 and 1.6 [45].

Two classes of materials of recent interests are skutterudites and clathrates; both have the ability to entrap ions or molecules within their crystalline lattice. There are two types of skutterudites, binary and ternary [46]. The first stoichiometrically consists of one cobalt, rhodium or iridium atom per phosphorous, arsenic or antimony atom [46]. The second is similar to the first with the exception that the cationic component is replaced with two ions whose averaged charges equal that of the binary cation [46]. Foreign ions can be placed into the empty spaces, or cages, within the crystal structure of the skutterudites for the enhancement of thermoelectric properties [46]. The highest reported *ZT* values for skutterudites in the publications reviewed are between 1 and 1.5 for temperatures between 700 and 1000 K [46]. Clathrates vary in crystal structure, but the better *ZT* values for clathrates have been around 0.3 for room temperature measurements and approach 1 above 700 K [47].

CHAPTER THREE

HYPOTHESIS AND OBJECTIVES

3.1 Hypothesis

The hypothesis of this thesis is that bismuth telluride nanowires can be grown electrochemically in porous anodic alumina membranes from aqueous nitric acid solutions that have been buffered with sodium hydroxide. Electrochemical deposition conditions affect crystalline structure and composition which in turn affect thermoelectric properties. By varying the pH of the deposition solution and the current supplied, a range of conditions under which aligned, bismuth telluride nanowires are grown can be found.

3.2 Objectives

This research is being funded by NASA and is part of an effort to develop an efficient thermoelectric device for cooling applications in space. In order to be effective in thermoelectric applications, the nanowires must meet the following objectives. The method for growing the nanowires must be able to be integrated into the device. The nanowires must be ordered and well aligned so that they can be part of the electrical circuit, and the materials and growth process should be compatible with the device. Samples of the nanowires must be characterized. Wire morphology, length, diameter, and growth density will be analyzed via electron microscopy. Composition will be elucidated through EDS and ICP.

CHAPTER FOUR

EXPERIMENTAL SET UP AND MEHTODS

4.1 Equipment

The equipment used in this investigation is listed in Table 3. The majority of the equipment and experiments performed were at NASA Ames Research Center at Moffett Field. The electrochemical deposition was performed with a potentiostat/galvanostat using General Purpose Electrochemical System (GPES) software with constant current settings. A Metrohm Ag/AgCl electrode was used for the reference electrode. A jacketed cell made in house was used during the depositions. The Innotech evaporator at Stanford Nanofabrication Facility was used along with the high resolution TEM with EDS at Stanford's Geballe Laboratory for Advanced Materials. The inductively coupled plasma-mass spectrometer (ICP) was operated by Dr. Paul Pak of the Department of Chemistry at San Jose State University.

Table 3. Equipment used in the electrochemical deposition of bismuth telluride.

Type	Manufacturer / Model	Specifications
Evaporator	Innotech ES26C	Electron beam source heating
Potentiostat/galvanostat	Autolab	GPES software
SEM	Hitachi S-4000	100,000x magnification
TEM with EDS	Philips CM20	200 keV; 1 to 2 Angstrom resolution
Reference electrode	Metrohm	Ag/AgCl
ICP II	Varian Liberty Series II	

4.2 Materials

The reagents used in the synthesis and harvesting of the nanowires are listed in Table 4. All of the reagents were purchased from Sigma-Aldrich.

Table 4. Chemicals used in the synthesis and harvesting of bismuth telluride nanowires.

Chemical	Purity	Form
$Bi(NO_3)_3 \bullet 5H_2O$	99.999 %	Pellets
Tellurium	99.997 %	40 mesh powder
Nitric acid, 70 %	99.999 %	Aqueous
Sodium hydroxide	99.99 %	Pellets

The AAMs were purchased from two manufacturers, Whatman and Synkera Technologies, Inc. Templates from both manufacturers were 13 mm in diameter and approximately 50 μm in thickness. The Whatman templates were actually sold as membrane filters under the name Anodisc 13. The specified 100 nm pore diameter were only valid for the very end of one side of the template; the bulk of the pores were actually closer to 200 nm in diameter. The specifications for the Synkera templates purchased are listed in Table 5.

Table 5. Specifications of nanoporous templates purchased from Synkera.

Part number	Pore diameter (nm)	Pore density (pores/cm^2)
OA-73-50-13 AAO	73 ±7	$4*10^9$
OA-55-50-13 AAO	55 ±6	$5*10^9$
OA-35-50-13 AAO	35 ±3	$1*10^{10}$
OA-13-50-13 AAO	13 ±2	$1*10^{11}$

The Whatman templates were used for preliminary experiments to gain an understanding of electrochemical deposition in pores. These templates were inexpensive

(~$2 per AAM) and purchased in excess. The Synkera templates were approximately ten times the price, depending on quantity purchased. As such, a limited amount of 73 and 55 nm pore-diameter templates were purchased, in conjunction with other groups at Ames, and only 5 of both the 35 nm and 13 nm pore diameter templates were purchased for some preliminary experiments. As such most of the depositions were performed with the two larger diameter templates, and the more rigorous and time consuming characterizations were performed on the wires grown in 55 nm pore diameter templates since thermoelectric enhancement is inversely proportional to wire diameter.

4.3 Procedure

The experimental procedure consists of four parts: the preparation of the working electrode, the preparation of the deposition solution, the electrochemical deposition, and the harvesting of the nanowires for characterization. Figures 4 and 5 are representations of the growth process and experimental apparatus used.

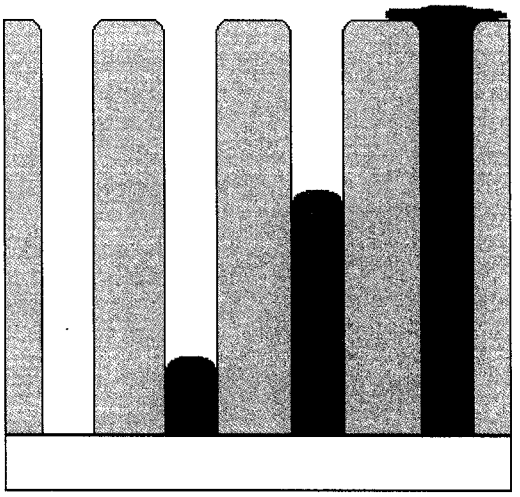

Figure 4. Illustration of electrochemical deposition into AAM.

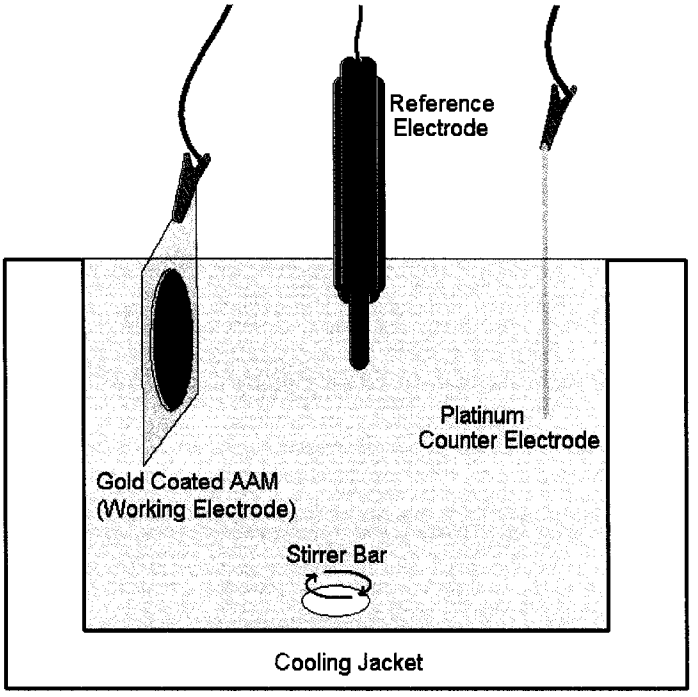

Figure 5. Electrochemical cell with cooling jacket. The cylindrical cell had an approximately 2.5 cm diameter base, was 5 cm tall, and was filled to about 4 cm.

The working electrode consisted of an AAM plated with gold that was pasted to a conducting surface. The Innotech electron beam evaporator at Stanford's

Nanofabrication Facility was used with standard operating procedures. Groups of as purchased AAMs were taped with minimal amounts of carbon tape to 4-inch silicon oxide on silicon wafers. Care was taken to avoid cracking or breaking the AAMs, and the pore diameters of the AAMs were scribed on to the wafers to avoid mix ups. The wafer on which the AAMs were taped and a couple of blank wafers were also coated with a 2 nm adhesion layer of titanium followed by a 200 nm layer of gold. As the pores had high aspect ratios, no significant amount of metal penetrated the pores.

When needed, the gold coated templates were removed from the wafer. The AAMs were adhered with colloidal silver paste to gold coated wafer pieces measuring approximately 1.5 cm by 4 cm so that an electrical connection existed between the gold films. The edges of the template and all but the top 1 cm of gold film were then coated with two layers of clear nail polish. This served as an insulating mask to prevent bismuth telluride from depositing on any exposed conductive surface.

Two solutions were made for electrochemical deposition by buffering a stock solution. The stock solution consisted of 5 M nitric acid in which tellurium powder and bismuth nitrate pentahydrate was dissolved to obtain the concentrations of 0.05 M Te^{+} and 0.035 M Bi^{3+}. Nitric acid released the toxic gas nitrogen dioxide upon contact with the metal, and as such, this step was performed in a fume hood. Batches of the final electrochemical deposition solution were made by taking aliquots of the stock solution and adding 1 M NaOH while monitoring the pH. Bismuth and tellurium ions formed gelatinous oxides during the preparation of pH 0.5-1 solutions. Subsequently, the precipitate was filtered out of the solution.

Bismuth telluride was deposited in the cell depicted in Figure 5. Approximately 20 ml of new deposition solution was used for each run. The solution was maintained at temperatures between 4 °C to 8 °C during the run with a cooling jacket. The solution was agitated with a magnetic stirrer bar set at 600 rpm. This speed provided for a highly stirred regime; essentially, this was the highest stirring rate (rounded down to the nearest hundred) achievable with the magnetic stirrer bar used. The electrodes used were a Metrohm Ag/AgCl reference electrode, a platinum wire counter electrode, and a gold backed AAM template which served as the working electrode. Prior to deposition, the template was soaked in the stirred, chilled solution for at least 2 hours for the Whatman templates and 24 hours for the narrower diameter Synkera templates. For deposition, the GPES software was set to apply a constant current for extended periods of time. The growth periods were not necessarily the same for each set of conditions or even between runs with the same sets of varied conditions. After deposition, the template was removed from the solution and rinsed with double distilled water.

While deposition can be crudely confirmed by visual inspection—templates turn black in areas with bismuth telluride—the wires must be separated from the template for characterization. For routine SEM, cross sections were obtained by simply breaking the templates in half while still adhered to the wafer piece; the wafer piece provided additional structural support.

Sample preparation for TEM analysis was significantly more challenging. The working electrode assembly was cleaned with acetone to remove the nail polish, to separate the template from the wafer piece, and to remove the colloidal silver particles

from the template. The template was then adhered to a clean wafer piece with Fix All Super Glue (only this type of adhesive was found to withstand the strongly alkaline conditions that followed). The template was then submerged in 10 ml of 5 M NaOH for at least four hours; the template was dissolved during this step, leaving the wires attached to the gold backing. The sample was then carefully rinsed with double distilled water several times followed by an overnight immersion in 10 ml of double distilled water and subsequent rinsing. The sample was then rinsed with isopropanol and placed in a 3 ml vial filled with isopropanol. The vial was sealed shut and sonicated for approximately 1 minute. A TEM copper grid was placed in the vial, and then the solution was shaken. Once particulates in the solution had settled, the TEM grid was removed, dried, and stored till TEM analysis.

For ICP analysis, the AAM template was similarly removed from the wafer piece, but the anodic alumina was not dissolved. Instead, the template was boiled in 70 percent nitric acid which selectively dissolves the bismuth telluride and leaves the gold and anodic alumina in tact. The standard solution consisted of 1 M HNO_3 with 52.5 ppm Bi^{3+} and 54.5 ppm Te^{2-} prepared from pure bismuth powders and tellurium powders. The operation and interpretation of ICP data were kindly performed by Prof. Paul Pak of the Department of Chemistry at SJSU.

For probe measurements, samples determined to have long nanowires (greater than 35 microns) were identified with SEM. The tops of the templates were sanded with scraps of polishing paper such that arrays of nanowires were exposed. With the existing gold working electrode serving as the contact on one side of the template, a second probe

was pressed upon the top of embedded nanowire arrays exposed at the other side of the template. The measurements were taken under the supervision of Dr. Toshige Yamada of NASA Ames Research Center who also graciously interpreted the results.

4.4 Experimental Program

Whatman Anodiscs of 200 nm nominal pore diameter were used for preliminary experiments prior to depositing into sub 100 nm templates. Two process parameters were varied at two levels for a 2^2 design of experiment matrix. As shown in Table 6, the factors of solution pH and applied current were chosen with pH values of 0.5 and 1, and -0.1 and -0.5 mA. These factors affected the composition, morphology and growth rate of the deposited material. The variables that were held constant include the concentrations of nitric acid, tellurium, and bismuth prior to the pH adjustment. The pH adjustment itself changed the concentrations of the components in the solution. The electrochemical cell's temperature, stirrer speed, approximate quantity of solution, and electrodes were also not varied. Depositions for each set of conditions were repeated at least three times, and each of these runs was analyzed with SEM. Further depositions and compositional analysis with ICP were performed on a selected run from each set of growth conditions.

Table 6. Experimental matrix for AAMs with diameters of 200 nm.

Number of Runs	pH	Applied Current (mA)
3	0.5	-0.1
3	0.5	-0.5
3	1	-0.1
3	1	-0.5

Using information obtained from the initial preliminary study, further depositions were investigated using the narrower diameter pores of Synkera templates with the pH 0.5 and 1 deposition solutions. Applied currents of -50 μA were used to deposit the nanowires in 73 and 55 nm pore diameter templates and -10 μA for 35 nm pore diameter templates. Depositions were attempted for templates with 13 nm pore diameters. SEM analysis was performed on all runs. As very few 35 nm and 13 nm pore diameter templates were available, less than ten depositions were attempted on these templates, and no further analysis was successfully completed. Also, only the 55 nm diameter templates were analyzed with ICP and TEM. It was the ultimate goal to synthesize and analyze as narrow a nanowire as possible, and sample preparation and analysis were very tedious and difficult for these nanowires.

CHAPTER FIVE

RESULTS AND DISCUSSION

5.1 Constant Current Electrochemical Deposition of 200 nm Diameter Wires

A preliminary investigation was performed using 200 nm pore diameter templates in anticipation of depositing bismuth telluride into AAMs with pores narrower than 100 nm. A two level, two factor design of experiment matrix was set up to test the effects of applied current and pH on the deposition of wires. Two solutions were prepared as previously described, a pH 0.5 solution and a pH 1 solution. Two current settings were applied during deposition, -0.1 and -0.5 mA. The different combinations of these conditions were repeated three times each, and the morphology of the nanowires from each run was observed. Additionally, compositional analysis was performed on selected runs.

Cross sections of arrays of wires in template were viewed under SEM to determine their morphology. Table 7 shows SEM images from several of these runs. Table 8 lists the growth rates of the wires. The growth rates were calculated by determining the average length of arrays of wires as viewed under SEM and dividing by the time a current was supplied.

Wires grown from one run under each set of conditions were selected for ICP analysis. The atomic percentage of bismuth for each of these runs is listed in Table 9, and the atomic percentage of tellurium is the balance out of 100 percent. The dissolved bismuth telluride wire solution for one of the runs was analyzed three times to investigate the reproducibility of the ICP reading.

Table 7. SEM images of wires grown in 200 nm diameter AAMs from several runs with pH 0.5 solution and -0.1 mA, pH 0.5 solution and -0.5 mA, pH 1 solution and -0.1 mA, and pH 1 solution and -0.5 mA.

Growth Conditions		SEM Images
pH	Current mA	
0.5	0.1	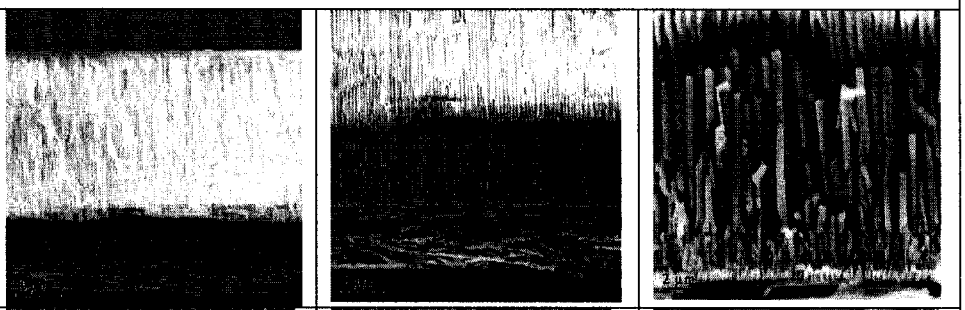
0.5	0.5	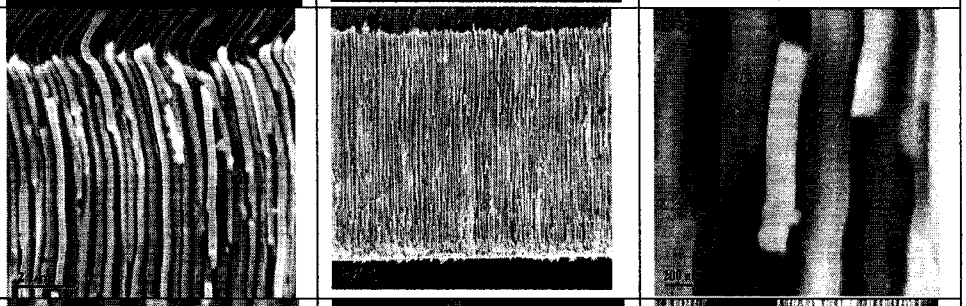
1	0.1	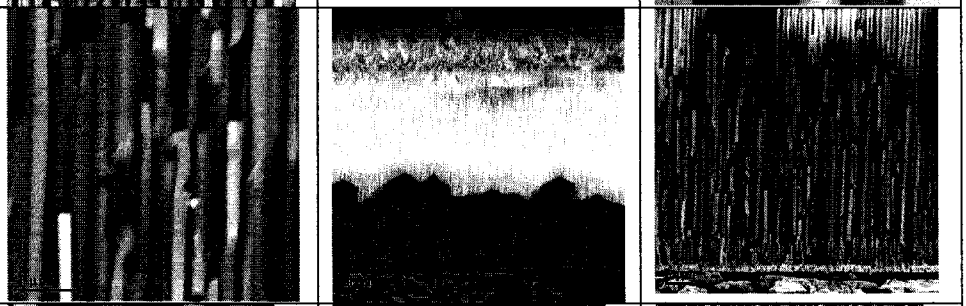
1	0.5	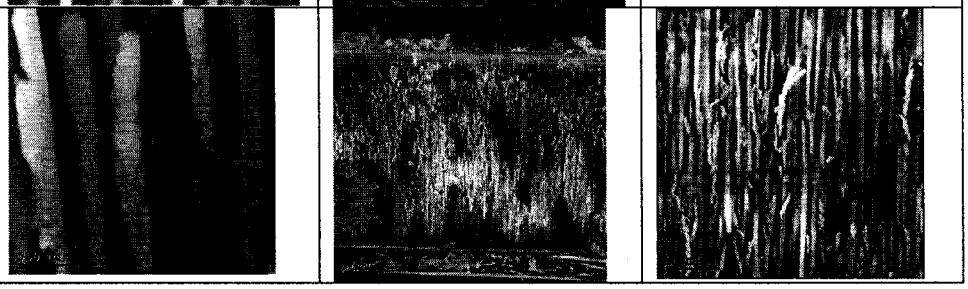

Table 8. Growth rates for arrays of 200 nm diameter bismuth telluride wires.

	Applied Current (mA)	Growth Rate (μm/hour)			
		Run 1	Run 2	Run 3	Average
pH 0.5	-0.1	0.5	1.1	1.0	0.9
	-0.5	3.1	3.1	3.2	3.1
pH 1	-0.1	0.6	1.3	0.5	0.8
	-0.5	5.8	4.8	4.0	4.9

Table 9. Atomic percentages of bismuth in Bi_xTe_{100-x} 200 nm wires as affected by pH and current during electrochemical deposition as determined by ICP.

	Applied Current (mA)	Atomic % Bismuth			
		Analysis 1	Analysis 2	Analysis 3	Average
pH 0.5	-0.1	39	--	--	39
	-0.5	36	--	--	36
pH 1	-0.1	25	--	--	25
	-0.5	17	15	15	16

5.1.1 SEM Analysis of 200 nm Diameter Wires

Two classes of wires are discernable through SEM imaging, high quality wires and low quality wires. High quality wires have smooth surfaces and completely wet the walls of the template. Low quality wires have rough, grainy surfaces and incompletely wet the walls of the pores. As the pore diameter was the upper limit for the wire diameter, the poor quality wires had narrower diameters in most regions than the high quality wires.

The wires that were grown with pH 0.5 solutions and with both current settings were found to be continuous with smooth surfaces as discernable with SEM. Similarly, wires that were grown with pH 1 solution and an applied current of -0.1 mA were found to be smooth. All runs under these three sets of conditions were therefore deemed to be

of high quality. The nanowires grown from the pH 1 solution at the higher current of -0.5 mA were not smooth and were composed of large grains. Some branching is even observed in the SEM images of the last row of Table 7. As such, the wires grown from each run with the higher pH and higher current were deemed low quality.

Serendipitously, it was found that applying a current density an order of magnitude above those used in the matrix study produced branched "nanotrees" as shown in Figure 6 for a pH 0.5 solution. Even higher current densities lead to gas elution and template explosion.

Figure 6. SEM image of bismuth telluride "nanotrees."

As these samples were made of high atomic number elements and were 200 nm in diameter, the as-grown samples were too thick to be analyzed with the TEM available. With the use of the SEM, the low quality wires can be easily dismissed as not being single crystalline; the multiple crystalline grains can be seen in the bumps and branches of the wires. For the high quality wires, single crystallinity is not ruled out, but further probing into the wire would be needed to prove this case. The growth of the 200 nm diameter wires was a preliminary investigation, and thermoelectric enhancement is not

expected for such large diameters even if TEM results indicated that the wires were defect free.

5.1.2 Composition of 200 nm Diameter Wires

The results of the ICP test shown in Table 9 should be taken as preliminary data. No other bismuth telluride nanowire studies reviewed report using ICP for compositional analysis. These measurements were taken as other characterization methods were both unavailable and not suited for the diameters of these wires. Repeat measurements were not taken, and statistical significance of the effects of the deposition parameters on wire composition cannot be distinguished.

For each deposition solution used, the higher currents lead to higher concentrations of tellurium deposited in the nanowires. And the depositions with the higher pH solution also lead to higher concentrations of tellurium than either of the currents with the lower pH solutions. The nanowires deposited with higher pH and more negative current deviated greatly from the 2 to 3 bismuth to tellurium stoichiometric ratio.

While all the depositions lead to tellurium rich alloys, the increase in tellurium with pH was not expected as the concentration of tellurium in the deposition solution actually decreases significantly with increasing pH. A log plot of the concentration of tellurium ions in equilibrium in aqueous solutions as a function of pH is given in Figure 7. This plot was adapted from the work of Pourbaix [49]. The solubility of bismuth should not be affected by the pH adjustments done to the deposition solution within the

range of concentrations and pHs used. There is some decrease in bismuth concentration as adding the 1 M NaOH to the 5 M HNO_3 solution with the dissolved bismuth and tellurium ions dilutes their concentration.

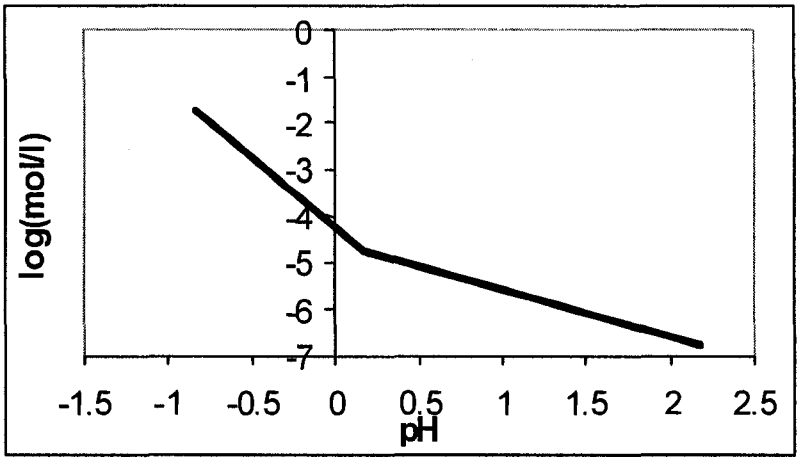

Figure 7. Log plot of tellurium solubility over a range of pH.

There are several variables that change with the addition of sodium hydroxide, not just the pH. One possible explanation for the decrease in bismuth concentration with increasing pH is the increase in viscosity with the addition of sodium hydroxide. In hindsight, it might have been more prudent to pick a different parameter to vary; this variable was chosen as this research largely followed the reports of Jin and coworkers and Li and coworkers who were the only ones to report single crystal wires and used pH 1 solutions [13, 14].

Should a method become available, it would be interesting to investigate whether phase separation had occurred for the samples that deviated greatly from the

stoichiometric ratio and had rough surfaces. The method used simply gives a percentage of all of the deposited material in the sample, not individual wires or sections of wire.

5.1.3 Effects of Electrodeposition Parameters for 200 nm Wires

Based on a survey of literature and preliminary experiments, sets of conditions were fixed or varied in this investigation. Beyond identical electrode fabrication, all of the runs had a degassing step, fixed stirrer speed, and deposition solution temperature between 4 to 8 ^{o}C. Prior to each run, each template was soaked in the deposition solution for 2 hours while the solution was stirred. This step ensured that all of the pores were filled with solution prior to the start of deposition. This was crucial for obtaining even growth. The stirrer was set to 600 rpm. This was just under the highest speed that the stirrer bar and plate could maintain for extended periods. A fast stirring rate was desired to keep the ion concentrations at the opening of the pores constant and to maintain a uniform temperature in the cell. The cell was maintained at 4 to 8 ^{o}C with a cooling jacket to slow the dissolution of the alumina templates as the runs were particularly long.

While the surfaces of the high quality wires are generally indistinguishable, the variation in deposition parameters did effect the growth of the wires, namely the growth rate. The growth rates were determined by taking the average length of the arrays of wires in a run and dividing by the deposition time. The average lengths of the wires was most easily determined for very uniform growth as seen in Figure 8(a) and approximated for less uniform runs, such as those from the pH 0.5, -0.5 mA runs. It should be noted that growth rates could not be taken for runs with over growth as it is not known when the wires reached the top of the template. Figure 8(b) shows one of the runs with over

growth. The duration of deposition was adjusted to avoid over growth but still obtain long enough wires for analysis.

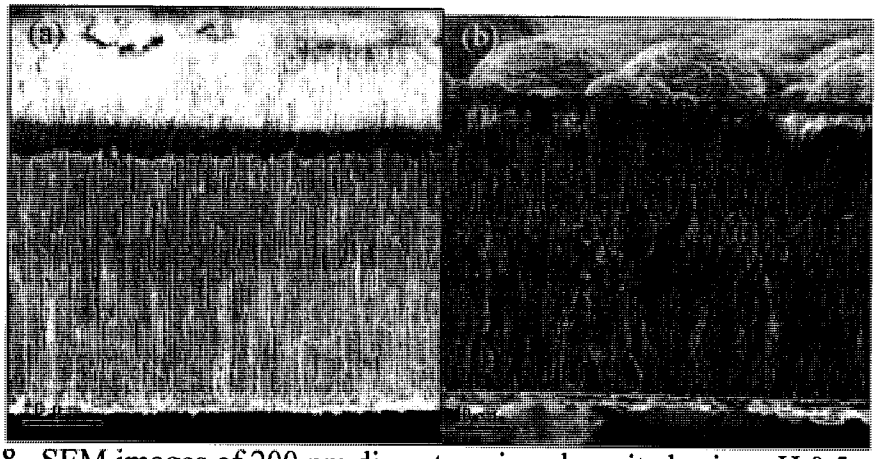

Figure 8. SEM images of 200 nm diameter wires deposited using pH 0.5 solutions. (a) Bismuth telluride wires exhibiting even growth with an applied current of -0.5 mA, and (b) overgrown wires grown using a current of -0.1 mA. Otherwise an annoying phenomena when imaging nonconductive materials such as alumina with electrons, the bright white blur at the top of (a) indicates that there is little or no conductive bismuth telluride. This is further indication of even growth.

For the high quality wires, the growth rate is roughly correlated to current density—which is different from the applied current. Optimally, the current supplied to each working electrode is distributed evenly across the entire conductive surface, and the current density is the applied current divided by the surface area of the electrode. For the working electrodes in these experiments, this surface area would initially be limited to the exposed gold film at the pore bottoms and would become the top surface of the bismuth telluride wires; the ratio of exposed conductive surface at the pore bottom to the total area of the exposed AAM including the non-conductive alumina is equivalent to the porosity of the membrane. Evidence for sufficiently distributed current would be a very high

percentage of pores with nucleated wires and even growth. Under the best conditions, the current density applied to the AAMs would be the total surface area of the unmasked AAM multiplied by the porosity. With 1 cm^2 unmasked surface areas and approximately 50 percent porosity, the current densities applied for these -0.1 mA and -0.5 mA runs would be -0.2 mA/cm^2 and -1 mA/cm^2, respectively. This is assuming complete pore nucleation, pore wetting and even growth.

A two-level, two-factor analysis of variance was performed to determine the effects of the varied parameters, pH and applied current, on the growth rate of the wires. The calculations for the analysis of variance are presented in Appendix A. The growth rate data used in the calculations are presented in Table 8. The different current settings, solution pH, and interaction of the two factors produced statistically significant growth rates with at least 95 percent confidence. The change in the applied current between -1 mA and -5 mA had the largest calculated F statistic value—an order of magnitude larger than the F statistic values—and the most pronounced effect on the growth rate. The pH and interaction effects were determined to be statistically significant. This was expected due to the appearance of a different deposition regime at the set of conditions with -0.5 mA and pH 1. This might not have affected the rate of deposition in terms of mass. The bismuth telluride did not deposit as densely in the pores as the material did not completely wet the pore walls.

As noted in Equation 2, electrons combine with the dissolved ions at the solution/growth interface to form the solid bismuth telluride. Thus, the higher growth rates occurred at higher applied currents. Between the two -0.5 mA growths, there is a

notable difference in growth rates. This can be attributed to the low quality of the pH 1, -0.5 mA wires. The low quality wires did not wet the pore walls and were thinner than the high quality wires. It is possible that comparable mass deposition rates occurred at the -0.5 mA level.

5.1.4 Implications for Electrodeposition into Nanoporous Alumina

As mentioned previously, the thermoelectric figure of merit is expected to increase with decreasing wire radii. Observations from the growth of 200 nm diameter wires were taken into consideration in the selection of the deposition parameters used with the templates with pore diameters less than 100 nm.

Degassing the pores by implementing a presoak step allows for a high percentage of wire nucleation and subsequent even growth. The importance of this step is underscored by the results from the DOE matrix runs. The applied current and hence the current density was shown to effect the growth rate and in one set of conditions, the deposition regime. Incomplete nucleation reduces the effective surface area and thereby increases the current density supplied to the open pores. Increased deposition rates at these pores would lead to faster wire growth rates and potentially overgrowth and the blocking of neighboring pores. Should a high enough current density be obtained at selected wires, poor quality growth or gas elution could occur.

Under uniform growth conditions, slower deposition has lead to the higher quality wires with higher amounts of bismuth. Cooler solution temperatures and buffered solutions retard the dissolution of the alumina template, allowing for longer runs. Li and

coworkers slowed the rate of deposition by having pauses in their deposition program; this pulsed voltage method was used with the idea that the ions depleted near the wire-solution interface would be able to be replenished during the pause [14]. The method investigated in the DOE matrix involved controlling the applied current, which under the high quality wire growth regime directly controlled the growth rate. At the lower currents, the diffusion of ions to the wire interface is thought to be fast enough to avoid significant depletion. The Synkera templates had lower porosity, and the need for smaller applied deposition currents was anticipated. Additionally, the narrower diameter pores would also slow the diffusion of the ions.

The pH of the deposition solution was also taken into consideration. The poor quality growth regime was repeatedly obtained with the pH 1 solution at the more negative applied potential tested in the DOE matrix. However, poor quality growth was also obtained with a pH 0.5 solution on a run in which the applied current was incorrectly set to a value that was approximately an order of magnitude more negative than the range tested in the matrix. This would indicate that the window for obtaining high quality nanowires would be narrower for the pH 1 solution. As single crystal bismuth telluride nanowires reported for pH 1 solutions in Li's and Jin's work, both pH levels were considered for the Synkera runs.

5.2 Constant Current Electrochemical Deposition of Nanowires

Bismuth telluride was deposited in 73 and 55 nm pore diameter Synkera templates using solutions buffered to pH 0.5 and 1, and it was also deposited into 35 nm pore

diameter Synkera templates using a pH 1 solution. Depositions in the 73 and 55 nm templates were run at -0.05 mA while the 35 nm templates were performed at -0.01 mA in order to avoid gas formation and poor quality growth. The porosity of the templates varied around 15 percent. However, the percentage of pore filling was less reproducible for these narrower diameter templates even with a minimum of 24 hrs of presoaking while monitoring the open circuit potential prior to deposition. While many runs resulted in high amounts of pore filling and even growth, there were also runs that did not, possibly due to template defects and contaminants on the working electrode/template interface. Table 10 summarizes the deposition conditions and the morphology of the nanowires produced.

Table 10. Qualitative results of electrochemical deposition of bismuth telluride into Synkera templates as determined by SEM.

Pore Diameter (nm)	pH	Current (mA)	Number of High Quality Runs	Number of Poor Quality Runs	Total Number of Runs
35	1	-0.01	2	1	3
55	0.5	-0.05	9	2	11
	1	-0.05	2	2	4
73	0.5	-0.05	6	0	6
	1	-0.05	2	1	3

Representative SEM images of the nanowires produced are shown in Figures 9-12. Figure 9 shows a 73 nm pore diameter template in which there was poor pore filling. The detail shows that there are also nanowires deposited that do not wet the pore walls

and have rough surfaces. Figure 10 (a) shows uniform nanowire growth from a pH 0.5 solution into a 73 nm pore diameter template. Figure 10 (b) shows freestanding nanowires from the same sample after the template has been dissolved away. Figure 11 shows a typical high quality deposition into a 55 nm pore diameter template. The higher magnification detail of Figure 11 shows two nanowires that have template induced defects which are different from the defects visible in Figures 6 and 9, and the bottom row of Table 7. The bismuth telluride in this deposition has wet the pore walls, completely filling the voids. However, as there are imperfections in the template, the deposited bismuth telluride takes the shape of this mold. Such defects were common in many of the Synkera templates of the various diameters. Figure 12 shows good quality 35 nm nanowires deposited from a pH 1 solution in template.

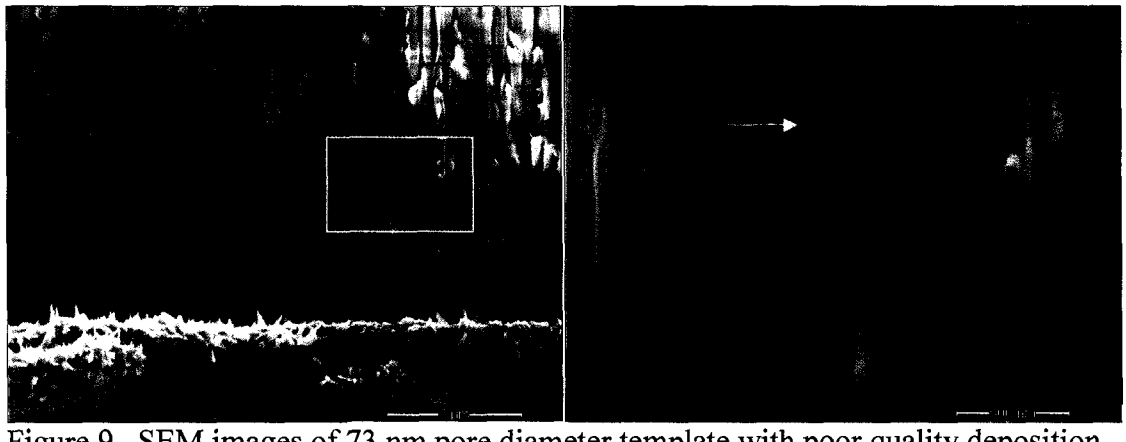

Figure 9. SEM images of 73 nm pore diameter template with poor quality deposition from a pH 1 solution.

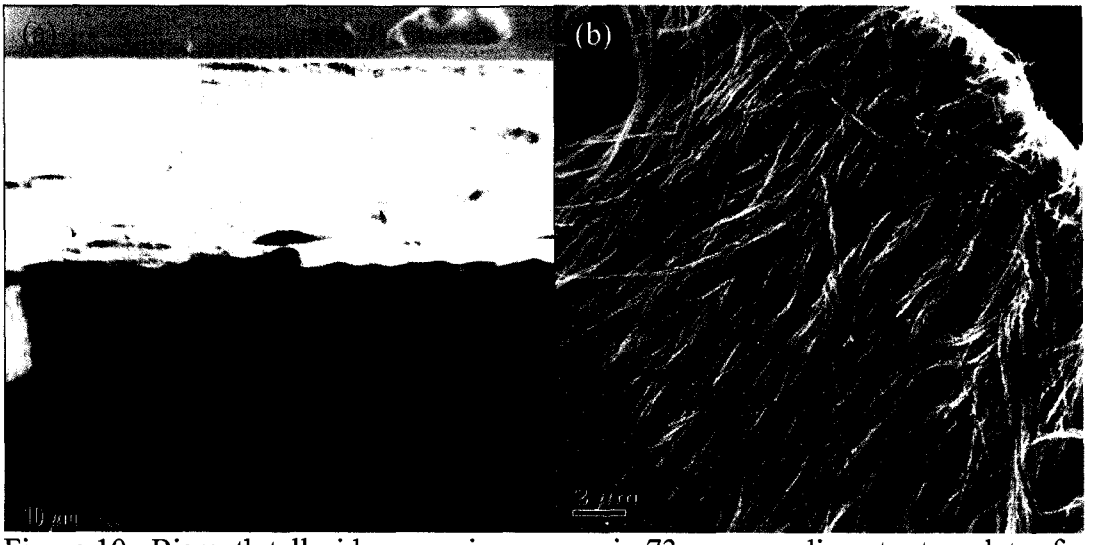

Figure 10. Bismuth telluride nanowires grown in 73 nm pore diameter templates from a pH 0.5 solution. (a) Nanowires in template with even growth, and (b) freestanding with template dissolved.

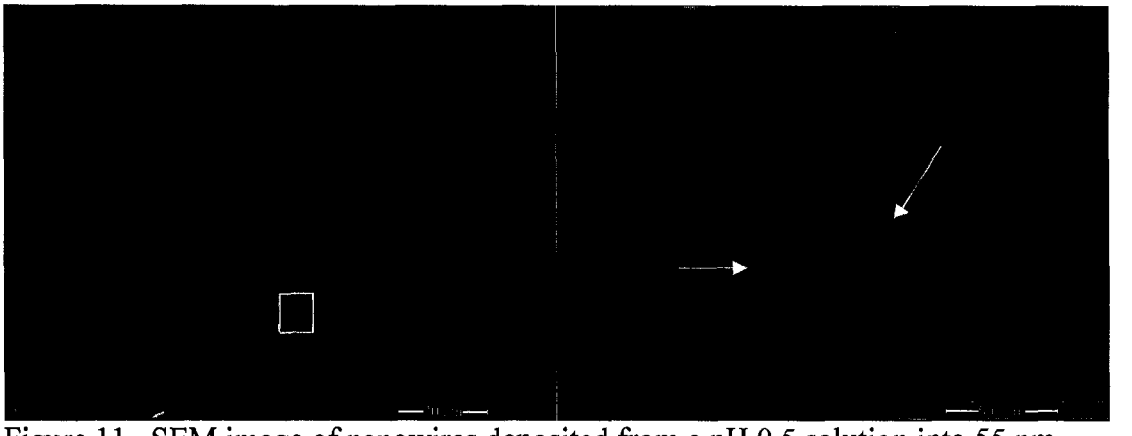

Figure 11. SEM image of nanowires deposited from a pH 0.5 solution into 55 nm diameter pores. The detail, the second image, shows template induced branching defects.

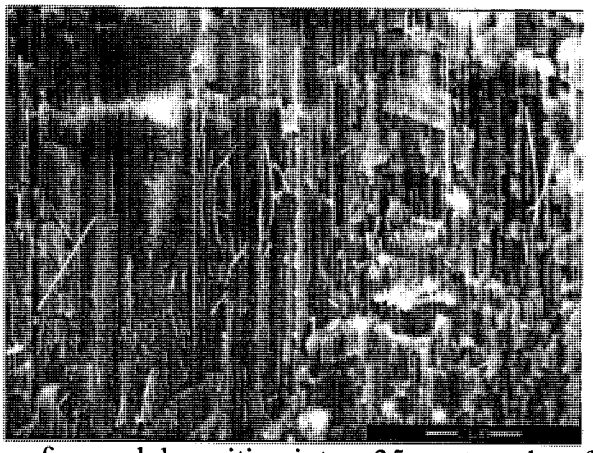

Figure 12. SEM image of a good deposition into a 35 nm template from a pH 1 solution and –0.01 mA applied current.

The growth rates of the nanowires in Synkera templates were not investigated as it was harder to determine the average length of the nanowires in each sample. The two main obstacles were difficulty imaging and uneven growth. The Synkera templates were not as porous as the Whatman templates, and the wires produced were much smaller. These two factors exacerbated the charging effects in the SEM, and imaging generally gets more difficult with decreasing dimensions. Even growth was harder to reproduce in the Synkera templates. The uneven growth made it difficult to determine an average nanowire length and sometimes lead to unexpected overgrowth.

After dissolution of the supporting anodic alumina, bismuth telluride nanowires from selected runs were cropped on TEM copper grids for analysis. The nanowires were found to be crystalline as shown in the HRTEM images in Figure 13 (a) and (b) for a nanowire 55 nm in diameter deposited from a pH 1 solution. Parallel lattice fringes are visible for the length of the nanowire imaged. The lattice spacing is 3.1 Å. Concentric beam electron diffraction patterns indicated that the nanowire is polycrystalline in nature,

as seen in Figure 13 (c). The EDX scan of the same nanowire, Figure 13 (d), revealed it to be tellurium rich when comparing the Bi_L and Te_L peaks.

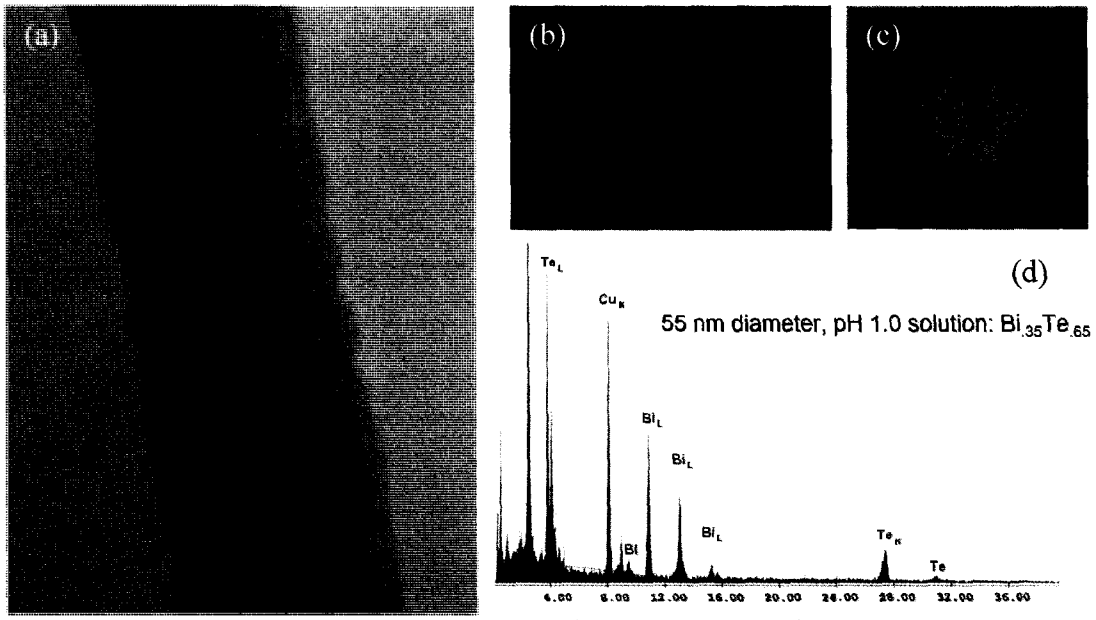

Figure 13. TEM analysis of a 55 nm nanowire. (a) HRTEM image of a 55 nm diameter nanowire, (b) HRTEM image of the same nanowire showing clear lattice fringes, (c) polycrystalline concentric beam electron diffraction pattern of the nanowire, and (d) EDX spectrum of this 55 nm nanowire.

Nanowires samples grown in 55 nm pore diameter templates and pH 0.5 and 1 solutions were analyzed with the TEM with EDX at Stanford's GLAM facility in a single session with the same TEM settings. Again, the Bi_L and Te_L peaks were analyzed. The atomic percentages of bismuth found in the samples are reported in Table 11. For the pH 1 sample, two wires were analyzed from the same run. Three separate scans were taken at adjacent sections along one of the wires. There was some variation between scans of the same wire. There are several possible reasons for compositional differences between wires with in the same run. These include the possibility of inhomogeneous deposition

conditions among the pores in the template and within various locations of the pores, as seen in the compositional changes along the same wire. Also, the samples had contamination from sodium hydroxide left from the template dissolution step. The sodium hydroxide, which is difficult to completely wash from the nanowires, might have interacted with the x-rays collected.

Table 11. As determined by TEM with EDX, atomic percentage of Bi in Bi_xTe_{100-x} nanowires as affected by the deposition solution. The wires analyzed were grown in 55 nm diameter pores with an -0.05 mA applied current.

Deposition Solution	Atomic % Bismuth	
	Wire 1	Wire 2
pH 0.5	25.5	--
pH1	16.6 17.7 19.1	13.1

Prior to the TEM EDX analysis, ICP compositional analysis was performed, largely because all other methods of analysis were not available at the time due to frequent and prolonged equipment failure. The compositions of arrays of nanowires grown in 55 nm diameter templates were analyzed. The effect of varying the pH of the prepared solution on the composition of the nanowires was tested and is shown in Table 12. Due to the reduced porosity and pore filling of the Synkera templates, these results had much smaller counts on the ICP. The reported percentages are more of an extrapolation from the calibration curve and should be considered less reliable than the 200 nm wire ICP results.

Table 12. As determined by ICP, atomic percentage of Bi in Bi_xTe_{100-x} nanowires as affected by pH and density during deposition.

Diameter (nm)	Deposition Solution	Current mA	Atomic % Bismuth	
			Run 1	Run 2
55	pH 0.5	-0.05	37	38
55	pH 1	-0.05	25	19

All of the nanowire samples were found to be tellurium rich. The cursory TEM EDX analysis and ICP analysis indicates the same trend as observed with the 200 nm diameter wires; the higher pH solution gives a more tellurium rich sample. However, the analysis methods give fairly different numbers. There are several reasons for this discrepancy. Namely, the ICP and TEM analyses were performed on different samples. The results of the TEM analysis shown in Figure 13 (d) differ from the TEM data displayed in Table 11 for the pH 1 deposition solution conditions, and these, again, are of different samples from different runs. Secondly, the ICP gives the atomic percentage of entire arrays of wires while the TEM gives a somewhat local measurement of one spot on a wire. Even within the same batch, the TEM shows different atomic percentages for different wires as seen between wires 1 and 2 for the pH 1 sample in Table 11.

5.3 Probe Measurements

Qualitative probe measurements were performed on arrays of nanowires embedded in the anodic alumina. Bismuth telluride nanowires grown with the pH 0.5 solution with 200 nm and 55 nm diameters were all found to be n-type. A V vs. log (I)

plot was made for an array of 55 nm nanowires and is shown in Figure 14. Also, all compositional analysis has indicates that all of the material deposited thus far would be n-type as it has been tellurium rich.

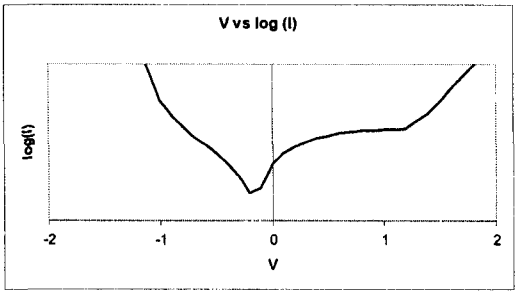

Figure 14. Probe measurement performed on an array of 55 nm nanowires deposited from a pH 0.5 solution demonstrating n-type behavior.

5.4 Pore Size and Template Considerations in Bi_2Te_3 Nanowire Deposition

As the figure of merit of a nanomaterial is expected to increase with decreasing dimensions, it was a goal of this investigation to deposit bismuth telluride into as narrow a pore as possible. The easiest deposition runs involved the 200 nm pore diameter templates. These templates required the shortest degassing time and shorter deposition times. Also, complete pore nucleation was observed for the majority of the runs attempted, and even growth was detected and repeated.

Depositions into the Synkera templates were significantly more difficult. The pores were a third of the diameter of the Whatman template or less. This lead to longer degassing times (minimally 1 day of soaking in the deposition solution) and longer deposition times at slower deposition rates. The good depositions were not consistently reproducible, and a definitive correlation between pore size, deposition conditions, and wire properties could not be established.

Pore size is not the only template characteristic to be considered in the selection of deposition conditions. As mentioned in the previous sections, the exposed conductive surface area is dependent upon the area of the unmasked template and the porosity of the template. The templates probably did not undergo the same anodization process to obtain the specified pore diameter and porosity. The templates were purchased from two different manufacturers, and the specific anodization conditions are not known. Different electrolyte solutions used in template preparation could have affected different surface characteristics for the alumina.

5.5 Further Investigations and Future Work

Beyond what has already been specified, several additional sets of conditions were attempted. These include investigations of variations in the deposition conditions and narrower diameter templates that did not result in nanowire growth. However, some insight was still gained from these trials. And this insight and the trends observed from successful bismuth telluride wire growth could be used in future investigations.

The experiments carried out using nitric acid solutions buffered with sodium hydroxide thus far have skewed towards being heavily tellurium rich and n-type. An aliquot of the stock 5 M HNO_3 solution was diluted to 1 M HNO_3 and an attempt to deposit into 55 nm diameter pores from an effectively pH 0 solution was made. From previous trends, it was thought that a higher bismuth concentration could be obtained. Due to the long exposure to the highly acidic solution, the template partially dissolved and broke apart. Buffering the deposition solution with sodium hydroxide had allowed

for longer runs with much less template dissolution. In general, more investigation of solution composition could be done to find the conditions necessary to obtain favorable p and n type carrier concentrations.

Templates with pores of 13 nm diameter were purchased from Synkera. These templates were prepared similarly as the other Synkera templates with larger pore diameters. The templates were soaked for at least two days in stirred electrochemical deposition solutions of pH 1 and pH 0.5. Constant current runs of -0.01 mA and constant voltage runs of -0.2 V and -0.15 V failed to produce nanowires. Additionally, application of the constant currents or voltages resulted in the decomposition of the template at the gold/alumina interface. No prior reporting of bismuth telluride nanowire electrochemical deposition below 20 nm had been found, and it is this range in which significant increases in *ZT* would are expected to occur for single crystal, optimally doped wires.

Only polycrystalline diffraction patterns have been observed in this study, and thermoelectric characterization of the nanowires, either individually or in arrays, has not been performed. Nanowires from this study had been sent to Dr. Li Shi's group at UT Austin. Due to the complexity and laborious preparation and the polycrystallinity of the nanowires grown, comprehensive measurements were not attempted. The crystalline grain boundaries and defects are expected to drastically reduce the electrical conductivity of the wires and thus decrease the *ZT*.

Overall, future work should include investigations leading to the formation of nanowires below 20 nm in diameter of single crystal quality. Two sets of conditions, each leading to p or n type material, need to be found with optimal carrier concentrations.

Thermoelectric characterization would need to be performed on these nanowires for feedback and to verify enhancement. This would have to be done on individual wires or on arrays of wires in the matrix. And ultimately, a complete thermoelectric device could be produced and tested using these new materials.

CHAPTER SIX

CONCLUSIONS

The goal of bismuth telluride nanowire research is to create working thermoelectric devices that would have much higher energy conversion efficiency than those current commercially manufactured. The improved device developed as a part of this project could be used to generate electricity from temperature gradients or in various cooling applications in space.

The approach used in this investigation was electrochemical deposition into nanoporous templates. This was chosen as there were previous reports on this method of synthesis, the chemicals used were relatively environmentally benign, and it is possible to fabricate devices using this method. The task of synthesizing nanowires is two fold as the final device would need arrays of p and n-type legs, both of single crystal quality and sufficiently narrow diameter. And for each type, the conditions for the optimal carrier concentration would need to be determined.

Bismuth telluride was deposited in 200, 73, 55 and 35 nm diameter pores to form arrays of submicron wires and three diameters of nanowires. In a two level, two factorial DOE matrix and in further nanowire growth, it was observed that increasing the applied current density increased the wire growth rate and the relative amount of tellurium in the resulting nanowire. It was also observed that increasing the pH of the deposition solution from 0.5 to 1 by adding sodium hydroxide led to relatively higher amounts of tellurium in the deposited nanowire. For the case of having both a high applied current and high pH, the wires grown turned out to have the highest concentration of tellurium and had rough

surfaces, large grains, and branches. These wires were easily determined to be polycrystalline. The crystallinity of the other wires with smooth surfaces was not investigated further as thermoelectric enhancement was not anticipated for such large diameters.

The information obtained from these depositions helped determine the parameters used in the deposition of nanowires 73, 55 and 35 nm in diameter. Depositing bismuth telluride into the nanoporous templates proved to be more tedious and less reproducible. However, dense arrays of nanowires of 73 nm and 55 nm diameters were deposited using pH 0.5 and 1 solutions, and 35 nm nanowire arrays were deposited using the pH 1 solution. TEM analysis revealed that even the smoothed surfaced 55 nm diameter nanowires were polycrystalline in nature and were tellurium rich. Probe measurements indicated that all sets of deposition conditions tested formed n-type material. The results of this study could be used in further attempts in obtaining single crystal bismuth telluride nanowires with optimal carrier concentrations.

REFERENCES

1. G.S. Nolas, J. Sharp and H.J. Goldsmid, Thermoelectrics: Basic Principles and New Materials Developments (Springer, New York, 2001) pp. 1-14.

2. M.S. Dresselhaus, Y.-M. Lin, O. Rabin, M.R. Black, S.B. Cronin and G. Dresselhaus, "*Overview of Bismuth Nanowires for Thermoelectric Applications,*" in Chemistry, Physics, and Materials Science of Thermoelectric Materials: Beyond Bismuth Telluride, edited by M.G. Kanatzidis, S.D. Mahanti, and T.P. Hogan (Kluwer Academic/Plenum Publishers, Boston, 2003) pp. 1-17.

3. H.W. Hillhouse and M.T. Tuominen, "*Modeling the Thermoelectric Transport Properties of Nanowires Embedded in Oriented Microporous and Mesoporous Films,*" Micropor. Mesopor. Mater., **47**, pp. 39-50 (2001).

4. T.K. Reynolds, J.G. Bales, R.F. Kelley and F.J. DiSalvo, "*The Synthetic Search for Better Thermoelectrics,*" in Chemistry, Physics, and Materials Science of Thermoelectric Materials: Beyond Bismuth Telluride, edited by M.G. Kanatzidis, S.D. Mahanti, and T.P. Hogan (Kluwer Academic/Plenum Publishers, Boston, 2003) pp. 19-34.

5. S.A. Sapp, B.B. Lakshmi and C.R. Martin, "*Template Synthesis of Bismuth Telluride Nanowires,*" Adv. Mater., **11**, pp. 402-404 (1999).

6. A.L. Prieto, M.S. Sander, M.S. Martin-Gonzalez, R. Gronsky, T. Sands and A.M. Stacy, "*Electrodeposition of Ordered Bi_2Te_3 Nanowire Arrays,*" J. Am. Chem. Soc., **123**, pp. 7160-7161 (2001).

7. M.S. Sander, A.L. Prieto, R. Gronsky, T. Sands and A.M. Stacy, "*Fabrication of High-Density, High Aspect Ratio, Large-Area Bismuth Telluride Nanowire Arrays by Electrodeposition into Porous Anodic Alumina Templates,*" Adv. Mater., **14**, pp. 665-667 (2002).

8. M. Martin-Gonzalez, G.J. Snyder, A.L. Prieto, R. Gronsky, T. Sands and A.M. Stacy, "*Direct Electrodeposition of Highly Dense 50 nm $Bi_2Te_{3-y}Se_y$ Nanowire Arrays,*" Nano Lett., **3**, pp. 973-977 (2003).

9. M. Martin-Gonzalez, A.L. Prieto, M.S. Knox, R. Gronsky, T. Sands and A.M. Stacy, "*Electrodeposition of $Bi_{1-x}Sb_x$ Films and 200-nm Wire Arrays from a Nonaqueous Solvent,*" Chem. Mater., **15**, pp. 1676-1681 (2003).

10. M. Martin-Gonzalez, A.L. Prieto, R. Gronsky, T. Sands and A.M. Stacy, "*High-Density 40 nm Diameter Sb-Rich $Bi_{2-x}Sb_xTe_3$ Nanowire Arrays*," Adv. Matter., **15**, pp. 1003-1006 (2003).

11. M.S. Sander, R. Gronsky, T. Sands and A.M. Stacy, "*Structure of Bismuth Telluride Nanowire Arrays Fabricated by Electrodeposition into Porous Anodic Alumina Templates*," Chem. Matter., **15**, pp. 335-339 (2003).

12. J. Keyani, A.M. Stacy and J. Sharp, "*Assembly and Measurement of a Hybrid Nanowire-Bulk Thermoelectric Device*," Appl. Phys. Lett., **89**, pp. 233206/1-233206/3 (2006).

13. C. Jin, X. Xian, C. Jia, W. Liu, W. Cai, L. Yao and X. Li, "*Electrochemical Fabrication of Large-Area Ordered Bi_2Te_3 Nanowire Arrays*," J. Phys. Chem. B, **108**, pp. 1844-1847 (2004).

14. L. Li, Y. Yang, X. Huang and G. Li, "*Pulsed Electrodeposition of Single-Crystalline Bi_2Te_3 Nanowire Arrays*," Nanotechnology, **17**, pp. 1706-1712 (2006).

15. W. Wang, Q. Huang, F. Jia and J. Zhu, "*Electrochemically Assembled P-Type Bi_2Te_3 Nanowire Arrays*," J. Appl. Phys., **96**, pp. 615-618 (2004).

16. X. Xu, L. Chen, C. Wang, Q. Yao and C. Feng, "*Template Synthesis of Heterostructured Polyaniline/Bi_2Te_3 Nanowires*," J. Solid State Chem., **178**, pp. 2163-2166 (2005).

17. J.R. Lim, J.F. Whitacre, J.P. Fleurial, C.K. Huang, M.A. Ryan and N.V. Myung, "*Fabrication Method for Thermoelectric Nanodevices*," Adv. Mater., **17**, pp.1488-1492 (2005).

18. W. Wang, F. Jia, Q. Huang and J. Zhang, "*A New Type of Low Power Thermoelectric Micro-Generator Fabricated by Nanowire Array Thermoelectric Material*," Microelectron. Eng., **77**, pp. 223-229 (2005).

19. L. Shi, C. Yu and J. Zhou, "*Thermal Characterization and Sensor Applications of One-Dimensional Nanostructures Employing Microelectromechanical Systems*," J. Phys. Chem. B, **109**, pp. 22102-22111 (2005).

20. E.J. Menke, M.A. Brown, Q. Li, J.C. Hemminger and R.M. Penner, "*Bismuth Telluride (Bi_2Te_3) Nanowires: Synthesis by Cyclic Electrodeposition/Stripping, Thinning by Electrooxidation, and Electrical Power Generation*," Langmuir, **22**, pp. 10564-10574 (2006).

21. Q. Wei and C.M. Lieber, "*Synthesis of Single Crystal Bismuth Telluride and Lead Telluride Nanowires for New Thermoelectric Materials*," Mat. Res. Soc. Symp. Proc., **581**, pp. 219-223 (2000).

22. A. Huczko, "*Template-Based Synthesis of Nanomaterials*," Appl. Phys. A, **70**, pp. 365-376 (2000).

23. H. Masuda and K. Fukuda, "*Ordered Metal Nanohole Arrays Made by a Two-Step Replication of Honeycomb Structures of Anodic Alumina*," Science, **268**, pp. 1466-1468 (1995).

24. P. Magri, C. Boulanger and J.M. Lecuire, "*Synthesis, Properties and Performances of Electrodeposited Bismuth Telluride Films*," J. Mater. Chem., **6**, pp. 773-779 (1996).

25. S. Michel, S. Diliberto, C. Boulanger, N. Stein and J.M. Lecuire, "*Galvanostatic and Potentiostatic Deposition of Bismuth Telluride Films from Nitric Acid Solution: Effect of Chemical and Electrochemical Parameters*," J. Crystal Growth, **277**, pp.274-283 (2005).

26. Y. Miyazaki and T. Kajitani, "*Preparation of Bi_2Te_3 Films by Electrodeposition*," J. Crystal Growth, **229**, pp. 542-546 (2001).

27. M. S. Martin-Gonzalez, A.L. Prieto, R. Gronsky, T. Sands and A.M. Stacy, "*Insights into the Electrodeposition of Bi_2Te_3*," J. Electrochem. Soc., **149**, pp. C546-C554 (2002).

28. B.Y. Yoo, C.-K. Huang, J.R. Lim, J. Herman, M.A. Ryan, J.-P. Fleurial and N.V. Myung, "*Electrochemically Deposited Thermoelectric N-Type Bi_2Te_3 Thin Films*," Electrochim. Acta, **50**, pp. 4371-4377 (2005).

29. W. Zhu, J.Y. Yang, X.H. Gao, J. Hou, S.Q. Bao and X.A. Fan, "*The Underpotential Deposition of Bismuth and Tellurium on Cold Rolled Silver Substrate by ECALE*," Electrochim. Acta, **50**, pp. 5465-5472 (2005).

30. M. Nedelcu, M. Sima, T. Visan, T. Pascu, I. Franga and F. Craciunoiu, "*$Bi_{2-x}Sb_xTe_3$ Thick Thermoelectric Films Obtained by Electrodeposition from Hydrochloric Acid Solutions*," in Proceedings of the XXth International Conference on Thermoelectrics, Beijing, China, 2001, pp.322-326.

31. D. Del Frari, S. Diliberto, N. Stein, C. Boulanger and J.-M. Lecuire, "*Comparative Study of the Electrochemical Preparation of Bi_2Te_3, Sb_2Te_3, and $(Bi_xSb_{1-x})_2Te_3$ Films*," Thin Solid Films, **483**, pp. 44-49 (2005).

32. Q. Ye, N. Mingo and L. Shi, "*Thermoelectric Nanowire Composites for Energy Efficient Refrigeration and Power Generation in Space Applications, Interim Review*," Unpublished talk a (September 2005).

33. R. Venkatasubramanian, P.J. Taylor, M.P. Walsh and B.E. LaForge, "*Thin-Film Thermoelectric Devices with High Room-Temperature Figures of Merit*," Nature, **413**, pp. 597-602 (2001).

34. R.F. Service, "*Thermoelectronics: Temperature Rises for Devices that Turn Heat into Electricity*," Science, **106**, pp. 806-807 (2004).

35. Y.Y. Zheng, T.J. Zhu, X.B. Zhao, J.P. Tu and G.S. Cao, "*Sonochemical Synthesis of Nanocrystalline Bi_2Te_3 Thermoelectric Compounds*," Mater. Lett., pp. 2886-2888 (2005).

36. X. Qiu, J.-J. Zhu, L. Pu, Y. Shi, Y.-D. Zheng and H.-Y. Chen, "*Size-Controllable Sonochemical Synthesis of Thermoelectric Material of Bi_2Te_3 Nanocrystals*," Inorg. Chem. Commun., **59**, pp. 319-321 (2004).

37. H.T. Zhang, X.G. Luo, C.H. Wang, Y.M. Xiong, S.Y. Li and X.H. Chen, "*Characterization of Nanocrystalline Bismuth Telluride (Bi_2Te_3) Synthesized by a Hydrothermal Method*," J. Crystal Growth, **265**, pp. 558-562 (2004).

38. X.H. Ji, X.B. Zhao, Y.H. Zhang, B.H. Lu and H.L. Ni, "*Synthesis and Properties of Rare Earth Containing Bi_2Te_3 Based Thermoelectric Alloys*," J. Alloys Compd., **368**, pp. 349-352 (2004).

39. N. Mingo, "*Thermoelectric Figure of Merit and Maximum Power Factor in III-V Semiconductor Nanowires*," Appl. Phys. Lett., **84**, pp. 2652-2654 (2004).

40. J.H. Seol, A.L. Moore, S.K. Saha, F. Zhou, L. Shi, Q.L. Ye, R. Scheffler, N. Mingo and T. Yamada, "*Measurement and Analysis of Thermopower and Electrical Conductivity of an Indium Antimonide Nanowire from a Vapor-Liquid-Solid Method*," J. Appl. Phys., **101**, 023706 (2006).

41. F. Zhou, J.H. Seol, A.L. Moore, L. Shi, Q.L. Ye and R. Scheffler, "*One-Dimensional Electron Transport and Thermopower in an Individual InSb Nanowire*," J. Phys.: Condens. Matter. **18**, pp. 9651-9657 (2006).

42. Q.L. Ye, T. Yamada, H. Liu, R. Scheffler, N. Mingo and R.L. Leverenz: "*Single Crystal InSb Nanowires: Synthesis, Characterization, Properties and Applications*," in Semiconductor Nanowires -- Fabrication, Physical Properties, and Applications, edited by V. Schmidt (Mater. Res. Soc. Symp. Proc. 940E, Warrendale, PA, 2006), Paper 0940-P07-05.

43. X. Zhang, Y. Hao, G. Meng and L. Zhang, "*Fabrication of Highly Ordered InSb Nanowire Arrays by Electrodeposition in Porous Anodic Alumina Membranes*," J. Electrochemical Soc., **152**, pp. C664-C668 (2005).

44. K.F. Hsu, S. Loo, F. Guo, W. Chen, J.S. Dyck, C. Uher, T. Hogan, E.K. Polychroniadis and M.G. Kanatzidis, "*Cubic $AgPb_mSbTe_{2+m}$: Bulk Thermoelectric Materials with High Figure of Merit*," Science, **297**, pp. 818-823 (2004).

45. T.C. Harman, P.J. Taylor, M.P. Walsh and B.E. LaForge, "*Quantum Dot Superlattice Thermoelectric Materials and Devices*," Science, **297**, pp. 2229-2232 (2002).

46. C. Uher, "*Structure-Property Relations in Skutterudites,*" in Chemistry, Physics, and Materials Science of Thermoelectric Materials: Beyond Bismuth Telluride, edited by M.G. Kanatzidis, S.D. Mahanti, and T.P. Hogan (Kluwer Academic/Plenum Publishers, Boston, 2003) pp.121-146.

47. G.S. Nolas, "*Clathrate Thermoelectrics,*" in Chemistry, Physics, and Materials Science of Thermoelectric Materials: Beyond Bismuth Telluride, edited by M.G. Kanatzidis, S.D. Mahanti, and T.P. Hogan (Kluwer Academic/Plenum Publishers, Boston, 2003) pp. 107-120.

48. D.-A Borca-Tasciuc, G. Chen, A. Prieto, M.S. Martin-Gonzalez, A. Stacy, T. Sands, M.A. Ryan and J.P. Fleurial, "*Thermal properties of electrodeposited bismuth telluride nanowires embedded in amorphous alumina*," Appl. Phys. Lett., **85**, pp. 6001-6003 (2004).

49. M. Pourbaix, Atlas of Electrochemical Equilibria in Aqueous Solutions, (Pergamon Press, New York, 1966) pp. 533-571.

50. M.R. Spiegel., Statistics, (McGraw Hill, New York, 1999) pp. 104-120.

APPENDIX A

ANALYSIS OF VARIANCE

Analysis of variance (ANOVA) is a standard statistical method that can be applied to analyze the significance of variables in a process. In this study, a two level, two factor design of experiments matrix was carried out with three sets of replications per set of conditions. The ANOVA equations for two treatments and two levels and three replications are given in Table 13. The growth rate data for bismuth telluride wires in the Whatman templates were obtained from Table 8. The calculated F statistic and intermediate values are presented in Table 14. The calculated F statistic values are compared with the tabulated F statistic for 1 and 8 degrees of freedom listed in Table 15. Conditions with calculated F statistic values larger the tabulated F statistic for the specified degrees of freedom are considered to significant with a certain percent of confidence.

The changes in the current and pH values of the deposition solutions had significant effects on the growth rates of the 200 nm wires. The current had the largest effect on the growth rate. Both changes and their interaction significantly effected wire growth rate at lest 95 percent confidence. These calculations are further discussed in the Results and Discussion section.

Table 13. Equations for two level two factor ANOVA with repeats [50].

	Variation	Mean Squares	Degrees of Freedom		F Statistic
Rows	$V_R = 2*3\sum_{j=1}^{2}\left(\overline{X}_{j\cdot\cdot} - \overline{\overline{X}}\right)^2$	$MSR = \frac{V_R}{1}$	1	8	$F = \frac{MSR}{MSE}$
Columns	$V_C = 2*3\sum_{k=1}^{2}\left(\overline{X}_{k\cdot\cdot} - \overline{\overline{X}}\right)^2$	$MSC = \frac{V_C}{1}$	1	8	$F = \frac{MSC}{MSE}$
Interaction	$V_I = 3\sum_{j,k}\left(x_{jk\cdot} - \overline{X}_{j\cdot\cdot} - \overline{X}_{k\cdot\cdot} + \overline{\overline{X}}\right)^2$	$MSI = \frac{V_I}{1}$	1	8	$F = \frac{MSI}{MSE}$
Residual	$V_E = \sum_{j,k,l}\left(x_{jkl} - \overline{X}_{jk}\right)^2$	$MSE = \frac{V_E}{8}$	1	8	

Table 14. Calculated F statistic for the effects of applied current and solution pH on the growth rates of bismuth telluride wires in 200 nm pore diameter templates. The F value for each of the variations between columns, rows, and runs is equal to its respective variation divided by MSE.

	Variation	Mean Squares	Degrees of Freedom		F Statistic Calculated
Current (Rows)	30.3	30.3	1	8	106.2
pH (Columns)	2.1	2.1	1	8	7.2
Interaction	2.6	2.6	1	8	9.2
Residual	2.3	0.3	1	8	

Table 15. Upper percentages for F distribution values corresponding to degrees of freedom of 1 and 8 [50].

Confidence	F Statistic
90 %	3.46
95 %	5.32
97.5 %	7.57
99 %	11.3